Energy jump during bond breaking

Naoki Miyazawa,* Masataka Hakamada, and Mamoru Mabuchi
Graduate School of Energy Science, Kyoto University, Yoshidahonmachi, Sakyo, Kyoto 606-8501, Japan
(Received 2 February 2017; revised manuscript received 22 June 2017; published 24 July 2017)

In current fracture theory, the fracture stress is related to the surface energy on the basis of linear elastic theory. However, the fracture stress does not necessarily exceed the stress required to break atomic bonds. Here, we show that a jump in the inelastic separation energy is generated by fracture, where the inelastic separation energy is the energy between the separation planes measured by excluding the contribution of elastic relaxation, and the stress at the onset of the energy jump is the fracture stress. Analysis of the electronic states of β-SiC (cubic SiC), Ge, and Cu by first-principles tensile tests shows that the electrons redistribute during surface formation in the transition from the onset to the end of the energy jump. Therefore, it is suggested that the inelastic separation energy at the end of the energy jump can be identified with the fracture energy. Also, first-principles shear tests show that an energy jump occurs during shearing for β-SiC, but not for Ge and Cu. Thus, an energy jump is a sign of fracture (bond breaking), and an energy jump during shearing is a good indicator estimating the ductile and brittle character. These principles can hold for any solid and will therefore be beneficial for the fundamental understanding of the mechanical properties of solids and for their industrial applications.

DOI: 10.1103/PhysRevB.96.014115

I. INTRODUCTION

Because unexpected fracture of structures can cause great damage, it is important to deeply understand the fracture mechanisms of solids. Pioneering work in the fracture theory of solids was performed by Griffith [1]. Analyzing fracture mechanisms from the macroscopic viewpoint based on linear elastostatics, he developed the concept of fracture stress as the balance between the release of strain energy and the increase of the surface energy when a crack grows. Strictly speaking, this fracture theory holds only for elastic materials, which fracture in a brittle fashion. However, it can be applied to deformable materials with ductile characteristics by considering the plastic zone around the crack tip [2]. The fundamental concept introduced by Griffith underlies modern fracture studies. However, there is no assurance that the fracture stress is related to the surface energy. Fracture of a solid is phenomenologically a discontinuous process because rigid surfaces are created. However, neither the fracture point nor the fracture energy can be strictly specified from the microscopic viewpoint because the inelastic energy between the separation planes (the inelastic separation energy), which is the separation energy measured by excluding the contribution of elastic relaxation, continuously changes with the separation distance, as described by, for example, the Lennard-Jones potential [3]. Moreover, linear elastostatics do not hold at the microscopic scale. Thus, understanding of the microscopic aspects of fracture in solids remains incomplete.

The ductility and brittleness are also the most important physical properties of solids. Several indicators of the ductile or brittle character of solids have been developed [4–12]. For example, Pettifor [13] investigated prediction of ductile and brittle character by the Pugh modulus ratio [4] and Cauchy pressure, and he succeeded in determining the character in several classes of materials, including intrinsically ductile ceramics. The Pettifor and Pugh criteria are based on the elastic properties. The γ_s/γ_{us} ratio, which is based on the inelastic properties, is another indicator of ductile versus brittle character [7], where γ_s is the surface energy and γ_{us} is the unstable stacking fault energy (USFE). In this case, a material must be sheared to a large strain to measure γ_{us}; for example, a large shear strain of 35% is needed to calculate γ_{us} for β-SiC (cubic SiC) [12]. However, practically brittle materials should be fractured before shearing to 35%. To avoid this irrationality, the fracture point must be specified.

In this paper, variations in energies as a function of strain were investigated for β-SiC, Ge, and Cu by relaxed-type and unrelaxed-type first-principles tensile tests. Here, β-SiC, Ge, and Cu represent typical covalently bonding semiconductor and metallic bonding materials, respectively. The β-SiC bulk crystal shows brittle behavior at room temperature [14]. Ge is plastically deformable at low temperature of 78 K [15]. From measurements of the Hall effect, it has been shown that the conductivity and lifetime of edge dislocations in Ge are associated with the acceptor-type energy levels in the middle or upper half of the gap [16]. Cu is typical of ductile metals.

II. METHODS

The first-principles tensile tests and the first-principles shear tests were performed on β-SiC, Ge, and Cu. The first-principles calculations were performed within the framework of density functional theory [17,18] as implemented in the CASTEP code [19]. The plane-wave basis set was used to calculate the electronic properties, and the generalized gradient approximation of the Perdew-Burke-Ernzerhof functional [20] was used for the exchange-correlation potential for the structure optimizations. Ultrasoft pseudopotentials [21] were used for all of the elements in the calculations. We applied cutoff energies of 280.0 eV for β-SiC, 180.0 eV for Ge, and 400.0 eV for Cu. The Brillouin zone was sampled using $8 \times 5 \times 1$,$6 \times 4 \times 1$, and $5 \times 6 \times 1$ Monkhorst-Pack k-point meshes [22] for β-SiC, Ge, and Cu, respectively. Periodic

*miyazawa.naoki.37c@st.kyoto-u.ac.jp

boundary conditions were applied in the x, y, and z directions for all of the calculations.

For β-SiC, Ge, and Cu, two types of first-principles tensile tests were performed, namely, relaxed-type and unrelaxed-type tests. The rectangular cell used for the two types of tensile tests contained 48 atoms, and it consisted of 12 layers of the (111) plane with a vacuum gap of 15 Å between periodically repeated slabs (see Supplemental Material, Figs. S1(a)–(c) [23]). In the relaxed-type tensile tests, after relaxing the cell, 1% incremental uniaxial tensile strain was applied to the crystal block in the ⟨111⟩ direction by separating the upper and lower halves of the crystal block such that the tensile direction was perpendicular to the slip plane [12]. In the calculations, the atoms located in the outermost two layers were fixed while the other atoms could freely move (see Supplemental Material, Fig. S2(a) [23]). After straining, the crystal block was relaxed based on Hellmann-Feynman forces until all of the forces were less than 0.03 eV/Å. The elastic strain energy generated by the applied tensile strain was stored in the cell. This step was iterated until fracture occurred. The unrelaxed-type tensile tests were performed to preclude generation of an energy jump. In the unrelaxed-type tensile tests, 1% incremental uniaxial tensile strain was applied to the crystal block by separating the upper and lower halves of the cell where all atomic positions were not relaxed, and this step was iterated until fracture occurred. The elastic strain energy was not stored in the cell in the unrelaxed tensile test because all atomic positions were fixed. The tensile directions for the unrelaxed-type tensile tests were the same as those for the relaxed-type tensile tests. The Poisson ratio was ignored to simplify the calculations. In addition, calculations were performed to measure the inelastic separation energy between the separation planes in the relaxed-type tensile tests (see Supplemental Material, Fig. S2(b) [23]). In the calculations, structure optimization was performed under the condition that movement of atoms located in the separation planes was fixed while the other atoms could freely move. In this way, the elastic strain energy stored in the cell was removed. Preliminary calculations were performed with a larger cell consisting of 18 layers to investigate the size effect. There were hardly any differences in the results between the calculations with a large and a small cell.

The first-principles fully relaxed tensile test was performed on a body-centered-cubic Fe $\Sigma 3$ (111)/[$\langle 1\bar{1}0\rangle$] tilt grain boundary (GB) segregated with H atoms. The cell used for the calculation contained 36 Fe atoms and two H atoms. The H atoms were placed at the interstitial site that was the most energetically stable site for H segregation [24–26], as shown in Supplemental Material Fig. S3(a) [23], on both sides of the Fe GB. The initial cell had dimensions of 0.405 × 0.702 × 1.489 nm. After relaxing the cell, 2% incremental uniaxial tensile strain was applied in the ⟨111⟩ direction (normal to the GB plane). All of the atoms were relaxed based on the Hellmann-Feynman forces until all the forces were less than 0.03 eV/Å. The lattice dimensions in the GB plane were fixed during the calculations, and the Poisson ratio was ignored to simplify the calculations [27–29]. This step was iterated until the GB fractured.

It is difficult to analyze the band structure of separation planes by first-principles calculations of multiple-layer cells. Thus, a two-layer cell was used to analyze the band structure of the separation planes, as shown in Supplemental Material Figs. S4(a) and (e) [23]. Unrelaxed-type first-principles tensile tests were performed for two-layer β-SiC and Cu, and the band structures were analyzed before deformation, at the onset point of breaking (OPB), and at the end point of breaking (EPB).

First-principles shear tests of pure alias shear [30] were performed. The rectangular cell used in the shear tests contained 48 atoms and consisted of 12 layers of the (111) plane (see Supplemental Material, Figs. S1(d)–(f) [23]). The top layer of the cell was displaced in the shear direction, such that the slip plane and the direction of the fault vector were (111) and $\langle 1\bar{1}0\rangle$ for β-SiC [12] and Ge [12], and (111) and $\langle 11\bar{2}\rangle$ for Cu [12], respectively. After displacing the top layer, the cell lengths, cell angles, and atomic positions were fully relaxed, except for the shearing angle and the atoms located in the top layer. This step was iterated until the displacement reached the length of the Burgers vector. In addition, calculations were performed to measure the inelastic separation energy between the shearing planes during pure alias shear. In these calculations, structure optimization was performed under the conditions that the positions of the atoms located in the shearing planes were fixed and the cell was fully relaxed. In this way, the elastic strain energy stored in the cell was removed.

Next, first-principles shear tests were performed on the cells used for the tensile tests. The upper and lower halves of the crystal blocks were displaced relative to each other along the fault vector within the slip plane until the displacement reached half of the Burgers vector, at which point the USFE was obtained. The atomic positions were relaxed only along the direction perpendicular to the slip plane. After the shear tests, the atoms were relaxed only along the direction perpendicular to the slip plane. Relaxed-type and unrelaxed-type first-principles tensile tests were then performed on the relaxed cells, in which the atoms were relaxed only along the direction perpendicular to the slip plane. In the calculations, the slip plane and the direction of the fault vector for the shear tests were (111) and $\langle 1\bar{1}0\rangle$ for β-SiC and Ge, and (111) and $\langle 11\bar{2}\rangle$ for Cu. The fracture plane and tensile direction for the tensile tests were (111) and ⟨111⟩ for β-SiC, Ge, and Cu, respectively.

III. RESULTS AND DISCUSSION

Figure 1 shows the variation in the total energy of the cell as a function of strain for the unrelaxed-type and the relaxed-type simulations. In the unrelaxed-type simulations, the separation planes moved along the tensile direction with all of the atoms fixed, and the inelastic separation energy between the separation planes was measured. In the relaxed-type simulations, only the atoms located in the top two layers of the cell were fixed for tensile straining, while the other atoms could freely move. The relaxed-type simulations correspond more closely to real tensile deformation. As shown in Fig. 1, in the unrelaxed-type simulations, the total energy continuously increases with the strain, although the rate of increase in the total energy is significantly reduced in a final stage. In the relaxed-type simulations, the change in the total energy is

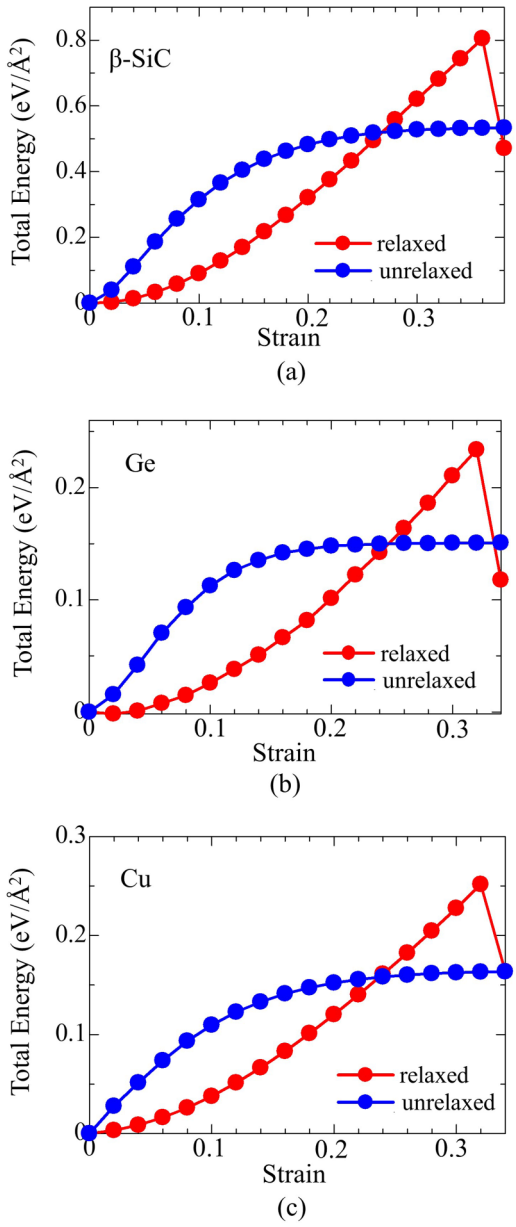

FIG. 1. Variation in the total energies of the (a) β-SiC, (b) Ge, and (c) Cu cells as a function of strain. The variation in the total energy was determined by relaxed-type and unrelaxed-type first-principles tensile tests. In the unrelaxed-type simulations, the separation planes move along the tensile direction with all of the atoms fixed. In the relaxed-type simulations, only the atoms located in the outermost two layers of the cell are fixed for tensile straining, while the other atoms can move freely. The total energy is found to continuously vary in the unrelaxed-type simulations. In the relaxed-type simulations, after the total energy continuously varies, it suddenly decreases in the final stage.

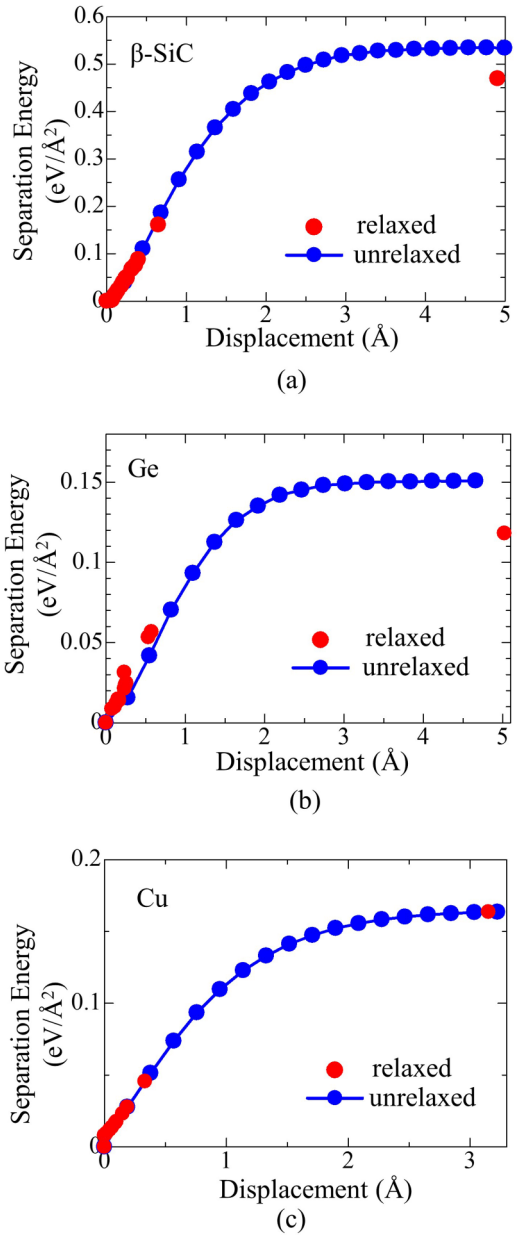

FIG. 2. Variation in the inelastic separation energy of the separation planes as a function of the displacement between them: (a) β-SiC, (b) Ge, and (c) Cu. The variation in the inelastic separation energy was determined by relaxed-type and the unrelaxed-type first-principles tensile tests. The inelastic separation energy continuously is found to vary in the unrelaxed-type simulations. In the relaxed-type simulations, the inelastic separation energy continuously varies until a certain displacement, and it then discontinuously jumps to its final value. The stress at the onset of the energy jump can be defined with the fracture stress. Although it appears that the number of data for the relaxed-type test is less than that for the unrelaxed-type test, some data for the relaxed-type test overlap, and the number of data for the relaxed-type test is the same as that for the unrelaxed-type test.

continuous, but there is a sudden decrease in the final stage. This discontinuity represents release of the elastic strain energy stored in the cell through fracture (bond breaking). The final values of the total energy for the two sets of simulations slightly differ, which is because of the small atomic movements in the separation planes by surface relaxation during deformation in the relaxed-type simulations [31].

Figure 2 shows the variation in the inelastic separation energy between the separation planes as a function of the displacement between the planes. The inelastic separation energy continuously varies in the unrelaxed-type simulations.

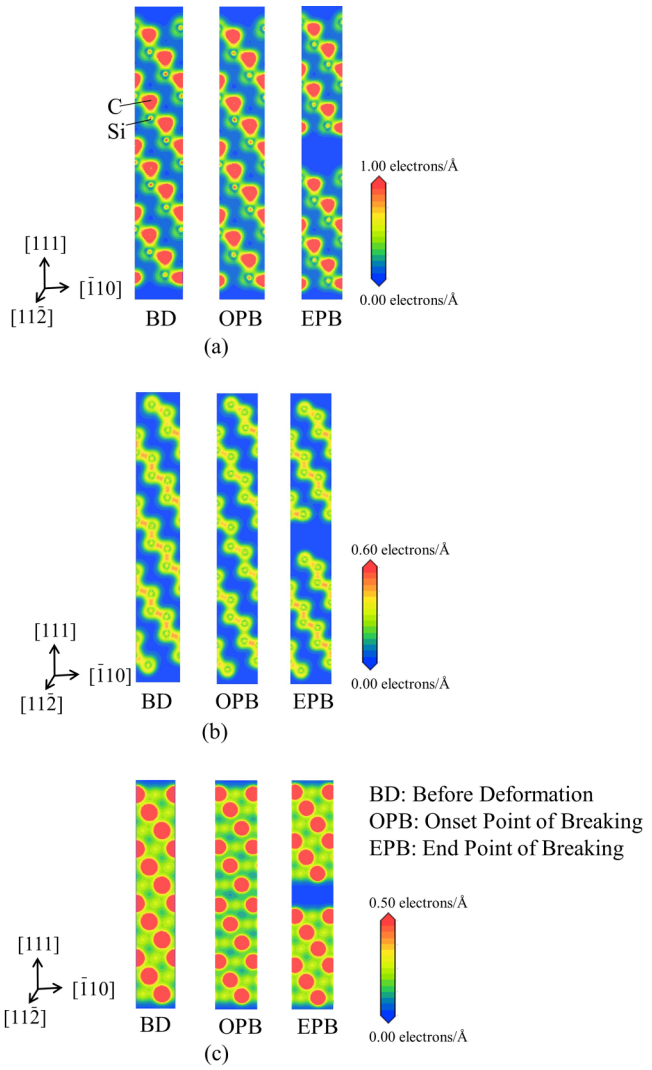

FIG. 3. Charge density distributions before deformation, at the OPB, and at the EPB: (a) β-SiC, (b) Ge, and (c) Cu. The charge density around the separation plane slightly decreases at the OPB compared with the charge density before deformation, but fracture is not completed at the OPB. On the other hand, the charge density around the separation plane decreases to zero at the EPB, which indicates that fracture is completed at the EPB.

Note that in the relaxed-type simulations, the inelastic separation energy continuously varies until a certain displacement, corresponding to the one in the unrelaxed-type simulations, but then discontinuously jumps to its final value. That is, a jump in the inelastic separation energy occurs, and an unstable transition state is generated during separation in the relaxed-type simulations. In this paper, the points just before and after the transition are termed the OPB and the EPB, respectively.

Figure 3 shows the charge density distributions before deformation, at the OPB, and at the EPB. It can be seen that the charge density around the slip plane slightly decreases at the OPB compared with that before deformation, but fracture is not completed at the OPB. On the other hand, the charge density around the slip plane decreases to zero at the EPB, which indicates that fracture is completed at the EPB.

Rose *et al.* [32] proposed the universal binding energy-displacement relation, which holds for a variety of materials [33–36]. According to the universal binding energy-displacement relation, the inelastic separation energy may be given by

$$E_{\mathrm{SR}}(x) = E_{\mathrm{SR},\infty}\left[1 - \left(1 + \frac{x}{l_b}\right)\exp\left(-\frac{x}{l_b}\right)\right], \qquad (1)$$

where E_{SR} is the inelastic separation energy per unit area, $E_{\mathrm{SR},\infty}$ is the inelastic separation energy when the displacement between the separation planes is infinitely large, x is the displacement between the separation planes, and l_b is the characteristic length scale at which maximum stress is obtained. The displacement at the OPB corresponds reasonably well with the displacement at which the maximum stress is obtained during the unrelaxed-type tensile tests, i.e., l_b (see Supplemental Material, Table S1 [23]). This indicates that the stress at the OPB is the fracture stress, which is given by $E_{\mathrm{SR},\infty}/(el_b)$ from Eq. (1). It is therefore considered that the transition from the OPB to the EPB is an unstable state in which the stress condition for fracture is satisfied, while the energy condition for fracture is not. The cohesive stress for cubic SiC was 47–58 GPa [37]. The fracture stress of $E_{\mathrm{SR},\infty}/(el_b)$ is calculated to be 49 GPa for SiC. Thus, the fracture stress of $E_{\mathrm{SR},\infty}/(el_b)$ well agrees with the cohesive stress. Also, the fracture energy can be specified as the inelastic separation energy at the EPB, which may be given by $E_{\mathrm{SR},\infty}[1-(1+a)/e^a)]$ ($a = l_s/l_b$, where l_s is the displacement at the EPB). If the applied load is stopped and no further energy for separation is supplied to a material during the transition state, the separation planes should return to their initial positions. However, in practice, because the strain energy stored in the cell is supplied to the material, fracture (bond breaking) may occur even if the applied load is stopped during the transition state.

The partial density of electronic states (DOS) of the atoms involved in bond breaking is shown in Fig. 4. The partial DOS at the OPB is similar to that before deformation, but the partial DOS significantly changes during the energy jump. The energy of smearing at a finite temperature is very small compared with the change in energy during the energy jump, and therefore the influence of smearing on the energy jump at a finite temperature is suggested to be negligible. The electrons are localized near the Fermi level at the EPB. This trend is particularly pronounced for β-SiC and Ge. Thus, the DOS at the Fermi level is increased by bond breaking [38]. It is known that impurity atoms, such as H, often induce GB embrittlement [39]. In such cases, the atomic bonds between impurity atoms and matrix atoms tend to preferentially break during straining. As an example of the cases, a H-segregated Fe GB was investigated by first-principles tensile tests. The DOS at the Fermi level for a Fe atom forming a Fe-H bond was found to increase by bond breaking (see Supplemental Material, Fig. S3 [23]). Thus, the same trend is found in the case of breaking of Fe-H bonds at a H-segregated Fe GB. In the case of the H-segregated Fe GB, only one Fe-H bond breaks and the other bonds do not, so there is no clear energy jump because the presence of nonbroken bonds obscures the energy jump which is related to bond breaking of Fe-H. As shown in Supplemental Material Fig. S3(b) [23], the bond

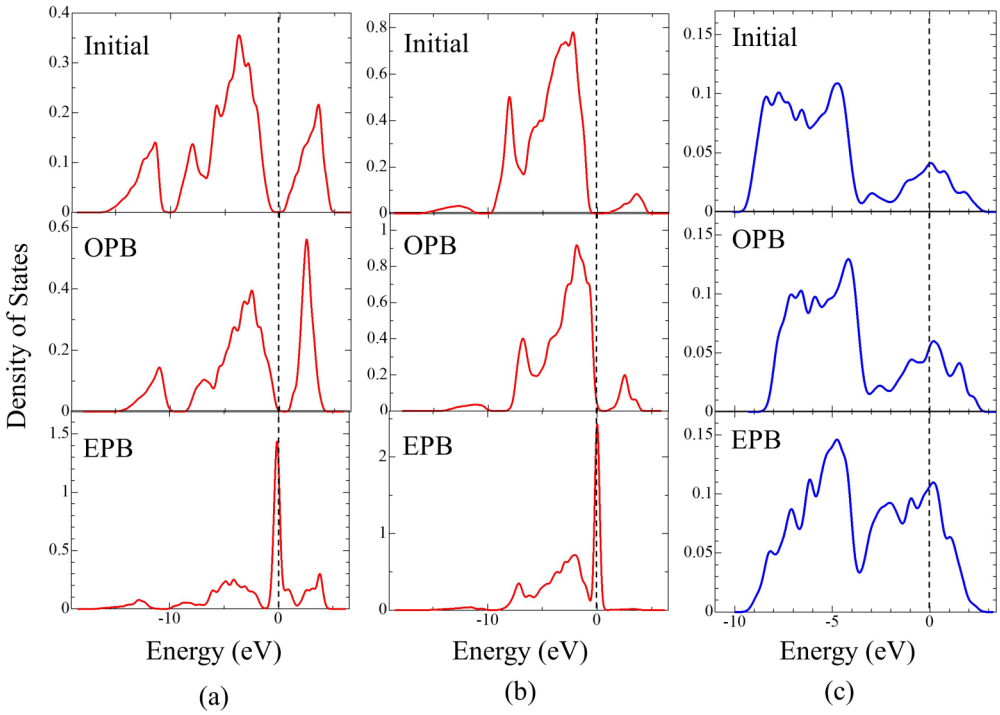

FIG. 4. Partial DOS before deformation (initial), at the OPB and at the EPB for β-SiC and Cu. (a) p orbitals of a Si atom, (b) p orbitals of a C atom, and (c) s orbitals of a Cu atom at the separation plane before deformation, at the OPB, and at the EPB. The partial DOS at the OPB is similar to that before deformation. The electrons are localized near the Fermi level at the EPB.

length of Fe-H suddenly increases. A jump in the energy can be identified by a sudden increase in the bond length because there is a one-to-one relation between the inelastic separation energy and the bond length. Therefore, an energy jump is suggested to be generated in the case of bond breaking of Fe-H.

A two-layer cell was used for band-structure analysis of the separation planes because it was difficult to analyze the band structure of separation planes by calculations with a cell consisting of many layers. In two-layer β-SiC and Cu, the band structure at the OPB is similar to that before deformation, while the electronic energies at the EPB tend to be discretized (see Supplemental Material, Fig. S4 [23]). Clearly, the jump in the inelastic separation energy is related to redistribution of the electrons during surface formation [40].

The energy at the OPB is quite lower than that at the EPB (see Supplemental Material, Table S1 [23]), which corresponds to significant redistribution of the electrons during the transition state. Notably, for Cu, the displacements at the OPB and EPB are the lowest among the materials investigated (see Supplemental Material, Table S1 [23]), in spite of the high ductility of Cu. Thus, ductile or brittle character cannot be estimated from the displacement at which bond breaking is induced. For Cu, the occurrence of bond breaking at smaller displacements may be because the electrons can easily redistribute because of the metallic bonding.

Figure 5 shows the variation in the inelastic separation energy between shearing planes as a function of the displacement determined by first-principles shear tests performing pure alias shear, where the displacement is the one between the shearing planes. The pure alias shear is a realistic description of shear deformation because the displacement propagates thorough the cell [30]. An inspection of Fig. 5 shows that the inelastic separation energy and the displacement significantly change during the period from the displacement of 0.83 Å to the displacement of 1.05 Å for β-SiC, but such significant changes are not found for Ge and Cu, indicating that a jump in the inelastic separation energy occurs for β-SiC before the inelastic separation energy reaches the USFE. This means that β-SiC fractured during shearing. Thus, β-SiC can be categorized as a brittle material because of the appearance of an energy jump. In contrast, there is no energy jump in the inelastic separation energy for Ge or Cu, suggesting that dislocations can glide on the slip plane without fracture, and thus Ge and Cu can be categorized as ductile materials. An energy jump occurs in the case of the onset of plastic deformation as well [41]. In this case, however, an energy is decreased by an energy jump because of the release of elastic energy. On the other hand, the inelastic separation energy is increased by an energy jump in the case of fracture during shearing because an energy jump occurs before the energy reaches the USFE.

We also investigated the variation of the inelastic separation energy during tensile deformation after shearing until the displacement at which the USFE was obtained (see Supplemental Material, Fig. S5 [23]). In the relaxed-type simulations, the inelastic separation energy jumps in the same manner as that shown in Fig. 2 for Ge and Cu. However, no jump occurs for β-SiC. The results support the view that an energy jump during deformation is a sign of fracture. In β-SiC, redistribution of the electrons during surface formation is completed during shear deformation. Therefore, no redistribution of the electrons

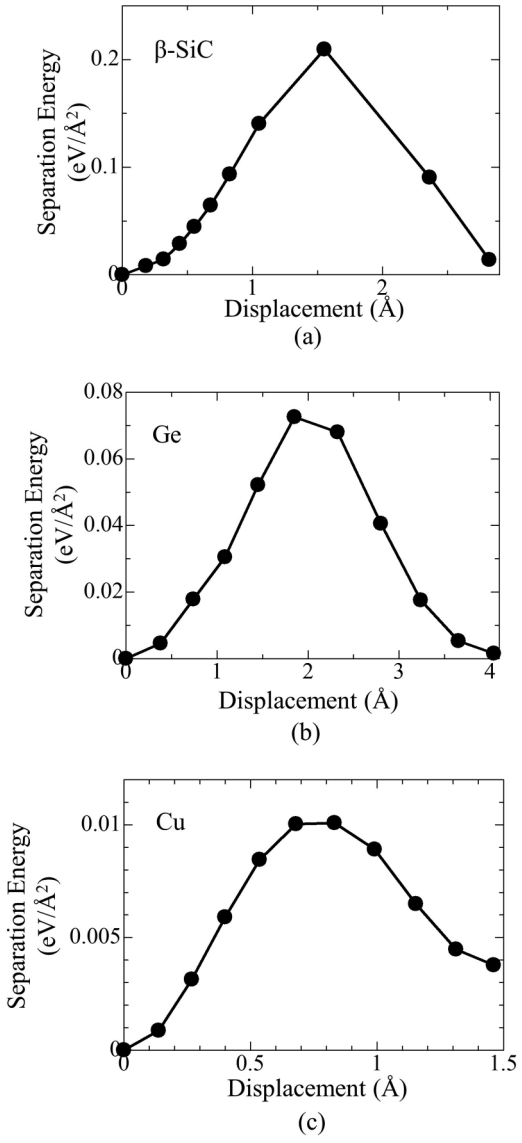

FIG. 5. Variation in the inelastic separation energy as a function of displacement for pure alias shear: (a) β-SiC, (b) Ge, and (c) Cu. The variation in the inelastic separation energy was measured by first-principles pure alias shear tests. A jump in the inelastic separation energy occurs for β-SiC before the inelastic separation energy reaches the USFE. No jump in the inelastic separation energy occurs for Ge and Cu.

occurs during tensile deformation after shear deformation, so there is no energy jump during tensile straining after shearing.

According to the virial theorem, the difference in the average total energy, consisting of the average total potential energy (PE) and the average total kinetic energy (KT), of the electrons before deformation and after fracture is given by

$$\langle E_{\mathrm{AF}}\rangle - \langle E_{\mathrm{BD}}\rangle = 1/2(\langle U_{\mathrm{AF}}\rangle - \langle U_{\mathrm{BD}}\rangle) = -\langle T_{\mathrm{AF}}\rangle + \langle T_{\mathrm{BD}}\rangle, \quad (2)$$

where $\langle E_{\mathrm{AF}}\rangle$ and $\langle E_{\mathrm{BD}}\rangle$ are the average total energies of the electrons after fracture and before deformation, $\langle U_{\mathrm{AF}}\rangle$ and $\langle U_{\mathrm{BD}}\rangle$ are the average total PEs of the electrons after fracture and before deformation, and $\langle T_{\mathrm{AF}}\rangle$ and $\langle T_{\mathrm{BD}}\rangle$ are the average total KTs of the electrons after fracture and before deformation, respectively. As shown in Fig. 4, the electrons at the EPB are in higher energy states than before deformation, although the electronic states at the OPB are similar to those before deformation. The displacement dependence of the PE is different from that of the KT. Therefore, it is suggested that the stress-displacement relation cannot be approximated by a function with symmetry, such as a sine curve, because redistribution of the electrons during surface formation leads to an increase in the average total PE of the electrons and a decrease in the average total KT of the electrons. Additionally, the emission of electrons and positive ions may occur during the transition state [42]. According to conventional fracture theory, the fracture stress satisfies the condition that the stress at the crack tip exceeds the ideal strength, assuming that the stress-displacement curve is approximated with a sine curve. However, it is not reasonable to approximate the stress displacement with a sine curve because the distribution of the electrons is fundamentally altered after the stress reaches the fracture stress, namely, an atomic bond reaches the OPB. Hence, the stress condition for bond breaking is not necessarily satisfied in conventional fracture theory.

IV. CONCLUSIONS

Relaxed-type and unrelaxed-type first-principles tensile tests have been performed on β-SiC, Ge, and Cu to investigate fracture from the microscopic view of bond breaking. The calculations showed that a jump in the inelastic separation energy is generated by fracture, and the electrons redistribute during surface formation in the transition from the onset to the end of the energy jump. In addition, the calculations suggested that the fracture stress can be identified with the stress at the onset of the energy jump, and the fracture energy can be identified with the inelastic separation energy at the end of the energy jump. Also, first-principles shear tests showed that an energy jump occurs during shearing for β-SiC but not for Ge and Cu. Thus, an energy jump during shearing is a good indicator for estimating the ductile and brittle character. The findings of this paper should be used for qualitative rather than qualitative understanding because of the limited number of atoms in the supercells.

ACKNOWLEDGMENTS

N.M. acknowledges support from the Grant-in-Aid for Japan Society for the Promotion of Science Fellows (Grant No. 16J11132).

[1] A. A. Griffith, Philos. Trans. R. Soc. Lond. A **221**, 163 (1921).
[2] G. R. Irwin, J. Appl. Mech. **24**, 361 (1957).
[3] J. E. Lennard-Jones, Proc. R. Soc. Lond. A **106**, 463 (1924).
[4] S. F. Pugh, Philos. Mag. **45**, 823 (1954).

[5] A. Kelly, W. R. Tyson, and A. H. Cottrell, Philos. Mag. **15**, 567 (1967).
[6] J. R. Rice and R. Thomson, Philos. Mag. **129**, 73 (1974).
[7] J. R. Rice, J. Mech. Phys. Solids **40**, 239 (1992).
[8] M. J. Mehl and D. A. Papaconstantopoulos, Phys. Rev. B **61**, 4894 (2000).
[9] U. V. Waghmare, E. Kaxiras, and M. S. Duesbery, Phys. Stat. Sol. (b) **217**, 545 (2000).
[10] T. Dasgupta, U. V. Waghmare, and A. M. Umarji, Phys. Rev. B **76**, 174110 (2007).
[11] S. Kamran, K. Chen, and L. Chen, Phys. Rev. B **79**, 024106 (2009).
[12] S. Ogata, J. Li, N. Hirosaki, Y. Shibutani, and S. Yip, Phys. Rev. B **70**, 104104 (2004).
[13] D. G. Pettifor, Mater. Sci. Technol. **8**, 345 (1992).
[14] C. Shin, H.-H. Jin, W.-J. Kim, and J.-Y. Park, J. Am. Ceram. Soc. **95**, 2944 (2012).
[15] W. Rindner and R. F. Tramposch, J. Appl. Phys. **34**, 758 (1963).
[16] G. L. Pearson, W. T. Read, and F. J. Morin, Phys. Rev. **93**, 666 (1954).
[17] P. Hohenberg and W. Kohn, Phys. Rev. **136**, B864 (1964).
[18] W. Kohn and L. J. Sham, Phys. Rev. **140**, A1133 (1965).
[19] M. C. Payne, M. P. Teter, D. C. Allan, T. A. Arias, and J. D. Joannopoulos, Rev. Mod. Phys. **64**, 1045 (1992).
[20] J. P. Perdew, K. Burke, and M. Ernzerhof, Phys. Rev. Lett. **77**, 3865 (1996).
[21] D. Vanderbilt, Phys. Rev. B **41**, 7892(R) (1990).
[22] H. J. Monkhorst and J. D. Pack, Phys. Rev. B **13**, 5188 (1976).
[23] See Supplemental Material at http://link.aps.org/supplemental/10.1103/PhysRevB.96.014115 for H-segregated Fe $\Sigma 3(111)$ grain boundary, band structures for two-layer β-SiC and Cu, tensile tests after shearing, simulation models, schematic illustrations of relaxed-type tensile tests, displacements and energy at OPB and EPB, and displacement at maximum stress.
[24] L. Zhong, R. Wu, A. J. Freeman, and G. B. Olson, Phys. Rev. B **62**, 13938 (2000).
[25] M. Yamaguchi, K.-I. Ebihara, M. Itakura, T. Kadoyoshi, T. Suzudo, and H. Kaburaki, Metall. Mater. Trans. A **42**, 330 (2011).
[26] Y. Itsumi and D. E. Ellis, J. Mater. Res. **11**, 2214 (1996).
[27] G.-H. Lu, S. Deng, T. Wang, M. Kohyama, and R. Yamamoto, Phys. Rev. B **69**, 134106 (2004).
[28] G.-H. Lu, Y. Zhang, S. Deng, T. Wang, M. Kohyama, R. Yamamoto, F. Liu, K. Horikawa, and M. Kanno. Phys. Rev. B **73**, 224115 (2006).
[29] Y. Zhang, G.-H. Lu, S. Deng, T. Wang, H. Xu, M. Kohyama, and R. Yamamoto, Phys. Rev. B **75**, 174101 (2007).
[30] M. Jahnátek, J. Hafner, and M. Krajcí, Phys. Rev. B **79**, 224103 (2009).
[31] T. D. Beaudet, J. R. Smith, and J. W. Adams, Solid State Commun. **219**, 43 (2015).
[32] J. H. Rose, J. R. Smith, and J. Ferrante, Phys. Rev. B **28**, 1835 (1983).
[33] P. Vinet, J. Ferrante, J. R. Smith, and J. H. Rose, J. Phys. C: Solid State Phys. **19**, L467 (1986).
[34] A. Banerjea and J. R. Smith, Phys. Rev. B **37**, 6632 (1988).
[35] R. L. Hayes, M. Ortiz, and E. A. Carter, Phys. Rev. B **69**, 172104 (2004).
[36] A. Srirangarajan, A. Datta, A. N. Gandi, U. Ramamurty, and U. V. Waghmare, J. Phys.: Condens. Matter **26**, 055006 (2014).
[37] L. Pastewka, A. Klemenz, P. Gumbsch, and M. Moseler, Phys. Rev. B **87**, 205410 (2013).
[38] J.-X. Shang and C.-Y. Wang, Phys. Rev. B **66**, 184105 (2002).
[39] M. Yuasa, T. Amemiya, and M. Mabuchi, J. Mater. Res. **27**, 1589 (2012).
[40] M. E. Eberhart, D. P. Clougherty, and J. M. MacLaren, J. Am. Chem. Soc. **115**, 5762 (1993).
[41] D. G. Sangiovanni, L. Hultman, V. Chiritra, I. Petrov, and J. E. Greene, Acta Mater. **103**, 823 (2016).
[42] J. T. Dickinson, E. E. Donaldson, and M. K. Park, J. Mater. Sci. **16**, 2897 (1981).